Regular Article

Au-Pd nanoparticles immobilized on TiO_2 nanosheet as an active and durable catalyst for solvent-free selective oxidation of benzyl alcohol

Zhe Wang [a], Jiangjiang Feng [a], Xiaoliang Li [a,⇑], Rena Oh [b], Dongdong Shi [a], Ouardia Akdim [c], Ming Xia [d], Liang Zhao [c], Xiaoyang Huang [c,⇑], Guojie Zhang [a,⇑]

[a] State Key Laboratory Breeding Base of Coal Science and Technology Co-founded by Shanxi Province and the Ministry of Science and Technology, Taiyuan University of Technology, Taiyuan 030024, Shanxi, PR China

[b] Department of Chemistry, Seoul National University, Seoul 08826, South Korea

[c] Cardiff Catalysis Institute, Centre for Doctoral Training in Catalysis, School of Chemistry, Cardiff University, Park Place, Cardiff CF10 3AT, United Kingdom

[d] State Key Laboratory of Coal Conversion, Institute of Coal Chemistry, Chinese Academy of Sciences, Taiyuan 030001, Shanxi, PR China

graphical abstract

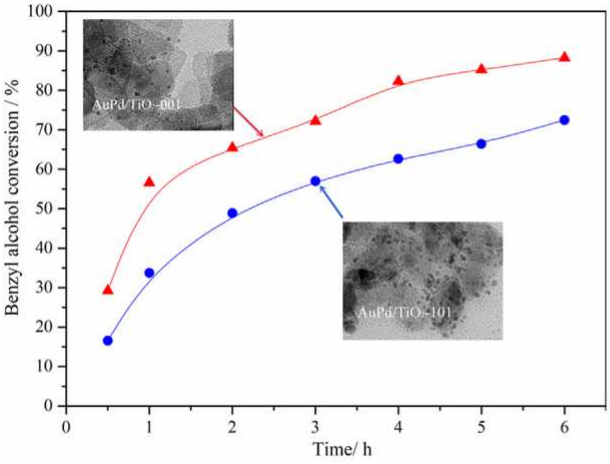

article info

Keywords:
AuPd NPs
TiO_2
Crystal facet engineering
Benzyl alcohol oxidation
Solvent-free

abstract

TiO_2 nanocrystals with controlled facets have been extensively investigated due to their excellent photo-catalytic performance in sustainable and green energy field. However, the applications in thermal catal-ysis without applying UV irradiation are comparably less and the identification of their intrinsic roles, especially the different catalytic behaviors of each crystal facet, remains not fully recognized. In this study, bimetallic AuPd nanoparticles supported on anatase TiO_2 nanosheets exposing {0 0 1} facets or TiO_2 nanospindles exposing {1 0 1} as a catalyst were prepared by sol-immobilization method and used for solvent-free benzyl alcohol oxidation. The experimental results indicated that the exposed facet of the support has a significant effect on the catalytic performance. AuPd/TiO_2-001 catalyst exhibited a higher benzyl alcohol conversion than that of the AuPd/TiO_2-101. Meanwhile, all the prepared AuPd/ TiO_2 catalysts were characterized by XRD, ICP-AES, XPS, BET, TEM, and HRTEM. The results revealed that the higher number of oxygen vacancies in TiO_2-sheets with the exposed {0 0 1} facets of higher surface energy could be responsible for the observed enhancement in the catalytic performance of benzyl alcohol oxidation. The present study displays that it is plausible to enhance the catalytic performance for the ben-zyl alcohol oxidation by tailoring the exposed facet of the TiO_2 as a catalyst support

⇑ Corresponding authors.
E-mail addresses: lixiaoliang@tyut.edu.cn (X. Li), HuangX17@cardiff.ac.uk (X. Huang), zhangguojie@tyut.edu.cn (G. Zhang).

1. Introduction

Selective oxidation of alcohols to aldehydes is a crucial reaction in both laboratory and industry. Aldehydes are critical chemical intermediates for the production of pharmaceuticals, fragrances, plastics, and fine chemicals et al. [1,2]. The traditional processes for benzaldehyde production involved chromates, permanganates, and peroxides together with organic solvents, which are not only expensive but also environmentally-unfriendly [3]. Hence, it is urgent to introduce molecular oxygen or compressed air as an oxi-dant to substitute the traditional stoichiometric oxidants in the selective catalytic oxidation of alcohol for green chemistry approach. Selective oxidation of benzyl alcohol to benzaldehyde is the typical oxidation reaction which is one of the most studied examples. In recent years, the catalytic oxidations of solvent-free benzyl alcohol with molecular oxygen as an oxidant have been widely reported [4–7]. Among the developed catalysts, Au-Pd based catalysts with different supports have attracted much more attention since the catalytic activity was enhanced by twenty-five-fold while retaining the same selectivity to benzaldehyde by alloy-ing Pd with Au, compared to the monometallic Au catalyst [4].

It is well known that the catalytic performance of the supported Au-Pd catalyst was closely related to the particle size, the nature of catalyst support, and the interaction between the noble metal and the support, together with the preparation method. As for the cat-alyst support, TiO_2 is a good candidate due to its chemical stability and the promising catalysis application [8], which has been widely used in photocatalytic hydrogen production [9–12], photocatalytic water splitting [13–15] and photocatalytic CO_2 reduction et al. [16–18]. Additionally, it also has been reported that Au-Pd nanoparticles supported on TiO_2 showed a high catalytic activity for benzyl alcohol oxidation [19]. It is generally accepted that the exposed facets of TiO_2 support also plays a key role in determining the catalytic activity, which inspired us to investigate the effect of the exposed crystal surface on the catalytic performance of AuPd/ TiO_2. TiO_2 nanosheets with a high percentage of reactive {0 0 1} facets have attracted much research attention in catalysis, which exhibited a higher surface energy (0.90 J/m^2) than most available anatase TiO_2 dominated by the thermodynamically stable {1 0 1} facets (0.44 J/m^2) [20]. Recently, the catalytic performances of TiO_2 nanosheet based catalysts have been reported in photocataly-sis and gas–solid heterogeneous catalysis, such as photocatalytic water splitting, photoreduction of CO_2 to CH_4, low-temperature CO oxidation, and selective catalytic reduction of NO_x with NH_3 et al. [21–24]. Furthermore, Pan et al investigated the photocat-alytic activity and stability of TiO_2 sheets for the benzyl alcohol oxidation in trifluorotoluene, which showed significant deactiva-tion [25]. However, the synthesized TiO_2 nanosheets as support for AuPd nanometallic catalyst have rarely been reported for ben-zyl alcohol oxidation. Based on which, it is essential to carry out the experiments to investigate the catalytic performance of Au-Pd nanoparticles immobilized on TiO_2 nanosheets for benzyl alco-hol oxidation.

In this work, TiO_2 nanosheets and nanospindles materials dom-inantly exposing the {0 0 1} and {1 0 1} facet, respectively, were pre-pared via the hydrothermal method with the assistance of structure-directing agent. Subsequently, Au-Pd nanoparticles were supported on the TiO_2 support by sol-immobilization method. The synthesized Au-Pd/TiO_2 catalysts were tested for the solvent-free benzyl alcohol oxidation in an aqueous phase. Meanwhile, XRD, ICP-AES, XPS, BET, TEM, EDS and HRTEM were conducted to char-acterize the prepared catalysts. The corresponding experimental results demonstrated that the as-synthesized Au-Pd/TiO_2 nanosheets catalyst showed high catalytic activity for benzyl alco-hol conversion and high selectivity towards benzaldehyde. The explanations on the catalyst structure–activity relationship were provided.

2. Experimental

2.1. Chemical materials

The chemical reagents were all purchased from Aladdin com-pany (Shanghai China) and used without any further purification: benzyl alcohol (99.8%, purity), $NaBH_4$ (98.0%, purity), PVA (Mw 31,000), $Ti(OBu)_4$ (99.0%, purity), TiO_2 (Degussa P25), HF (40.0%, purity), CH_3COOH (99.8%, purity), $PdCl_2$ (99.999%, purity), and $HAuCl_4$ $3H_2O$ (99.9%, purity). O_2 (99.999%, purity) was sup-plied from Taiyuan iron and steel corporation.

2.2. Preparation of the catalyst support

Anatase TiO_2 sheets were prepared using hydrothermal method based on Xie's report [26]. Basically, 25 mL of $Ti(OBu)_4$ and 3 mL of 40 wt% HF were mixed in a 100 mL Teflon autoclave and then kept stirring at room temperature for 30 min. Then the autoclave was put in an oven and kept at 180 ⅬC for 24 h under the static state. After being naturally cooled to room temperature, the white pro-duct was collected by filtration and washed with deionized water and ethanol for three times, respectively, followed by drying at 90 ⅬC for 18 h in an oven. Anatase TiO_2 spindles were also synthe-sized by employing the hydrothermal method with the assistance of structure-directing agent CH_3COOH [23]. 10 mL of $Ti(OBu)_4$ was mixed with 40 mL of CH_3COOH (without 40 wt% HF) in a 100 mL Teflon-lined autoclave and the mixed solution was maintained at 200 ⅬC for 24 h in an oven. After cooling down to room tempera-ture, the precipitate was centrifuged, washed with water, and then dried at 90 ⅬC for 18 h. The obtained TiO_2 sheets and spindles were denoted as TiO_2-001 and TiO_2-101, respectively.

2.3. The immobilization of Au-Pd nanoparticles on TiO_2

Au-Pd/TiO_2 (TiO_2 sheets, spindles and P25) catalysts with Au:Pd mass ratio of 1:1 were prepared by the sol-immobilization method [27]. In a typical preparation procedure, 1.00 mL of $HAuCl_4$ solution (5 mg Au/mL) and 1.00 mL of $PdCl_2$ solution (5 mg Pd/mL) were added into 100 mL of de-ionized water and the mixed solution was kept stirring at room temperature for 15 min. The PVA solu-tion was subsequently added with the mass ratio of PVA to Au + Pd of 1.2. Then, the required amount of the freshly prepared $NaBH_4$ solution with the molar ratio of $NaBH_4$ to Au + Pd of 5.0 was immediately added into the above mixed solution to form a dark-brown solution. After stirring for 30 min, 0.99 g of the pre-pared TiO_2 or commercial TiO_2-P25 was added and the pH of the mixed solution was adjusted to 1 by sulfuric acid under vigorous stirring conditions. After 1 h, the products were filtered, washed with deionized water and dried at 110 ⅬC for 18 h in an oven.

The final AuPd/TiO_2 sheets and AuPd/TiO_2 spindles were denoted as AuPd/TiO_2-001 and AuPd/TiO_2-101, respectively.

2.4. Benzyl alcohol oxidation

The benzyl alcohol catalytic oxidation was conducted in a 50 mL glass-lined min claves (Anhui Kemi machinery Technology Co., Ltd, China). Firstly, the autoclave was charged with 15 mL of benzyl alcohol and 0.03 g of catalyst before it was purged five times with oxygen. Subsequently, the reactor was pressurized to 0.3 MPa with O_2 at room temperature. The reaction mixture was heated to the required temperature at 1000 rpm. The reactor was also connected with the oxygen reservoir for the purpose of replenishing the consumed oxygen during the reaction. The reaction products were analyzed by GC (FuLi GC9790, Zhejiang, China) equipped

with a flame ionization detector (FID) and DM-5 column (30 m 0.25 mm 0.25 lm).

The benzyl alcohol conversion X and the TOF values were calcu-lated as follows:

$$X = \frac{\delta n_{benzylalcohol;in} - n_{benzylalcohol;out}}{n_{benzylalcohol;in}} 100\%;$$

$$TOF = \frac{n_{benzylalcohol;in} X}{\delta n_{Au} + n_{Pd} \cdot t} ;\delta X \leq 15\%$$

'n' is the molar mass; 't' is the reaction time.

2.5. Catalyst characterizations

ICP-AES was conducted on an Agilent 735-ES instrument. Powder XRD (PXRD) was performed on a Rigaku D/max-RC diffrac-tometer with CuKa radiation at 40 kV and 25 mA (k = 0.15418 nm). X-ray photoelectron spectroscopy measurements were carried out on a PHI-1600ESCA System XPS spectrometer (Perkin-Elmer, USA) using non-monochromatic Mg-Ka radiation. TEM and HRTEM were performed by JEM-2100 electron microscope operating at 200 kV. STEM-EDS mapping was carried out on a FEI Titan Cubed Themis G2 300 aberration-corrected scanning transmission electron microscope manipulated at 300 kV. N_2-BET surface area was deter-mined by using Micrometrics ASAP 2020. UV–vis absorption spec-troscopy was operated by Cary 60 UV/vis spectrophotometer.

3. Results and discussion

The synthesized TiO_2-001 and TiO_2-101 materials were charac-terized by TEM and HRTEM, and the results were shown in Fig. 1. In detail, Fig. 1a1 and b1 displays the different morphologies between TiO_2-001 and TiO_2-101, i.e. sheet and spindle, respectively. Fur-thermore, TiO_2-001 and TiO_2-101 exhibited clear lattice fringes with an interplanar distance of 0.24 nm and 0.35 nm correspond-ing to {0 0 1} facets and {1 0 1} facets, respectively, which reveals that both supports were synthesized successfully exposing a single facet as designed. Meanwhile, HRTEM-EDS were analyzed for the catalysts after AuPd nanoparticles immobilized, where signals of both Au and Pd were observed, indicating the AuPd nanopartilces were well deposited onto the prepared supports, see Fig. S1 in SI.

Fig. 2 shows the XRD patterns of the bare TiO_2 and AuPd/TiO_2 samples. We obtained eight peaks positioned at 2h = 25.3L, 36.9L, 37.8L, 38.6L, 48.0L, 53.9L, 55.2°, and 62.7L, which were indexed to (1 0 1), (1 0 3), (0 0 4), (1 1 2), (2 0 0), (1 0 5), (2 1 1), and (2 0 4) crystal facets of the anatase TiO_2 (PDF No.21-1272), respectively [28]. This demonstrates the successful synthesis of TiO_2 with pure crystalline phase. Apparently, the (0 0 4) diffraction peaks of TiO_2-001 and AuPd/TiO_2-001 are broader than the TiO_2-101 related catalysts, sug-gesting the massive appearance of (0 0 1) facets [29]. Similarly, the (1 0 1) diffraction peaks of TiO_2-101 and AuPd/TiO_2-101 are broader than the TiO_2-001 related catalysts, which indicates the massive appearance of (1 0 1) facets instead. Furthermore, AuPd/TiO_2-001 and AuPd/TiO_2-101 have displayed the same patterns as their bare supports, which implies that the crystal structure and crystal size of TiO_2 were not affected by the introduction of AuPd nanoparticles. The crystalline phase including Au and Pd were not detected from XRD patterns, which is consistent with their microscopic results of particle size smaller than 5 nm (Fig. 4). Besides, specific surface area

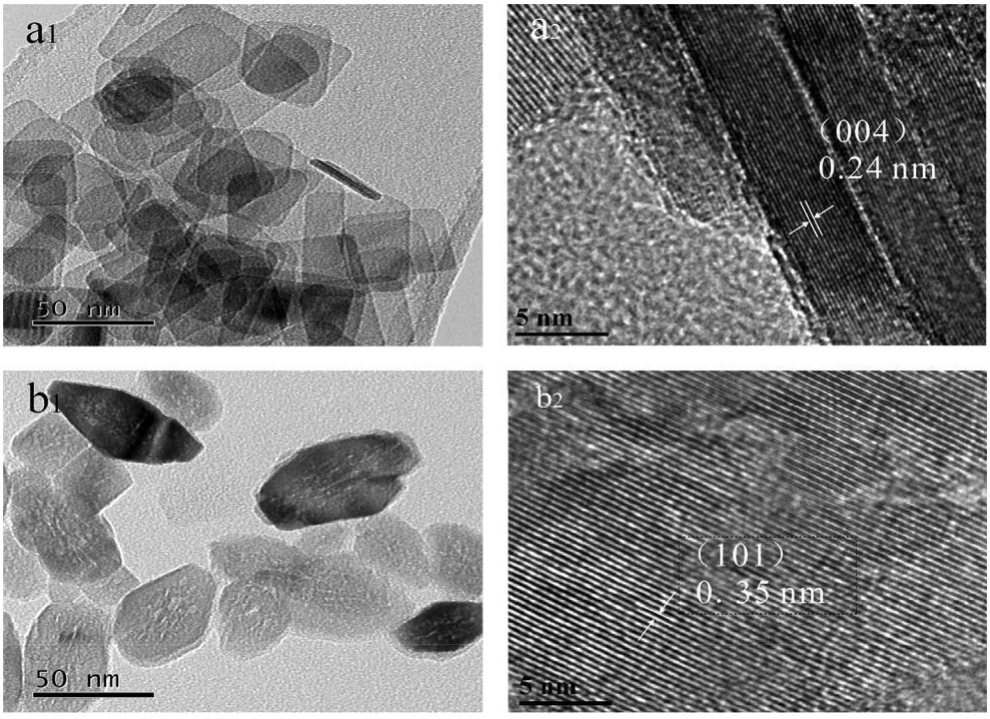

Fig. 1. TEM and HRTEM images of TiO_2 nanosheets (a_1, a_2) and TiO_2 nanospindles (b_1, b_2).

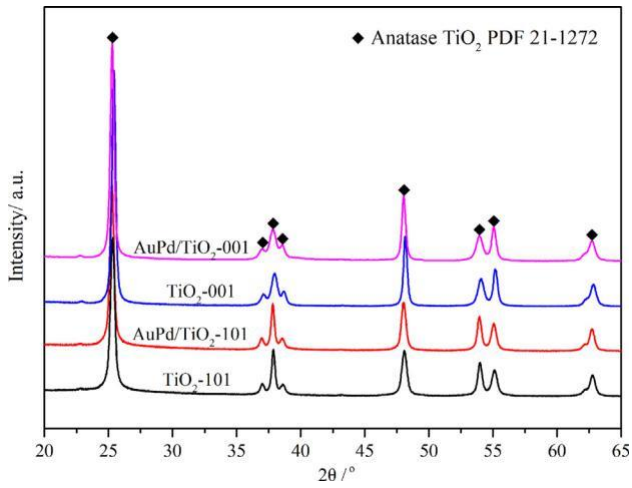

Fig. 2. XRD patterns of series of TiO_2 and their corresponding AuPd/TiO_2 catalysts.

of both supports were determined according to Brauner-Emmet-Teller (BET) method, which is 68 m^2/g and 54 m^2/g for TiO_2-001 and TiO_2-101, respectively. The AuPd/TiO_2-001 and AuPd/TiO_2-101 catalysts were determined to possess specific surface area of 64 m^2/g and 51 m^2/g, respectively.

The prepared AuPd/TiO_2 catalysts in this study have a nominal metal loading of 1.0 wt% with the Au/Pd mass ratio of 1:1. ICP-AES was conducted to determine the actual concentrations of Au and Pd in the catalysts. The corresponding results were summarized in Table S1 in SI, which demonstrated that >96% of Au and Pd were successfully anchored on the catalyst surface. The difference between the nominal and actual metal concentration might be attributed to the measurement deviation and the leaching of the weakly adsorbed AuPd during the catalyst preparation [30].

XPS was performed to identify the chemical states of Au, Pd, Ti and O in AuPd/TiO_2-001 and AuPd/TiO_2-101 and the corresponding results were exhibited in Fig. 3. The Au 4f spectra displays two peaks of Au $4f_{5/2}$ and $4f_{7/2}$ located at 87.2 eV and 83.5 eV, while the characteristic positions of the spin–orbit split peaks for metal-lic Au are 87.7 eV and 84.0 eV [4]. The 0.5 eV shift towards to a lower binding energy could be interpreted as a result of charge transfer from Pd to Au since Au is more electronegative than Pd [31–34]. For Pd 3d two characteristic peaks positioned at 340.9 eV and 335.6 eV corresponding to $3d_{3/2}$ and $3d_{5/2}$ were observed, showing that Pd(0) was incorporated in AuPd alloy, instead of Pd (II) species. In literature, the metallic Pd has its 3d region with peaks fitted at 340.4 eV and 335 eV [35], however in our work the shift of ca 0.5 eV to higher binding energy was observed, which can be an additional indication of the electronic interaction between Au and Pd. Thereby, upon the XPS results, it is proposed that Au and Pd are alloyed to each other for both

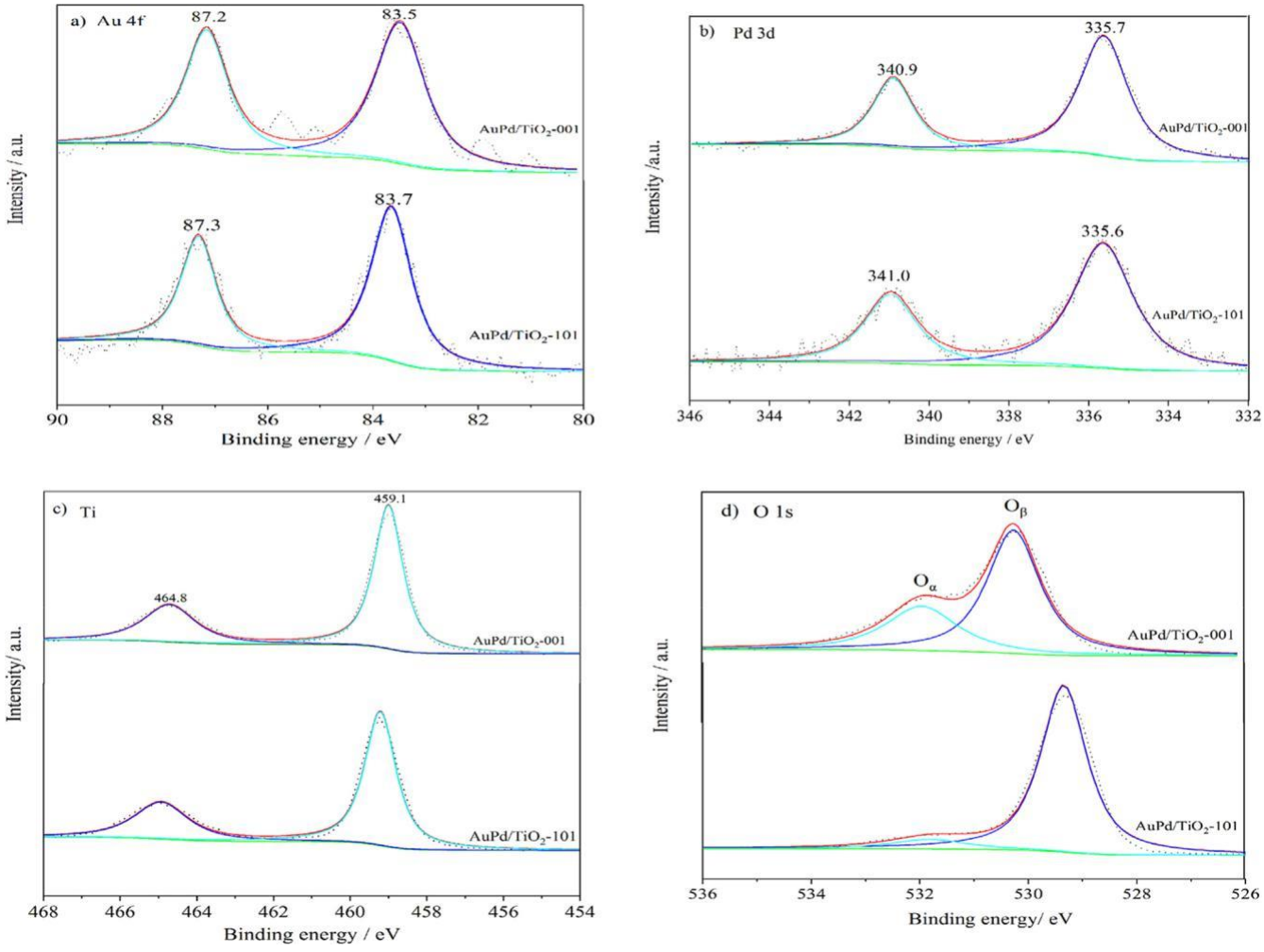

Fig. 3. XPS spectra of Au 4f (a), Pd 3d (b), Ti 2p (c) and O 1s (d) for AuPd/TiO_2-001 and AuPd/TiO_2-101 catalysts.

AuPd/TiO_2-001 and AuPd/TiO_2-101 catalysts [36]. Furthermore, O1s shows a significant different signal between two catalysts. The peak located at 529.3 eV and 531.9 eV were assigned to oxygen in TiO_2 lattice (signed as O_b) and oxygen vacancy (signed as O_a), respectively [32]. It is noteworthy that AuPd/TiO_2-001 exhibited a higher value of $O_a/(O_a + O_b)$ (32.8%) compared to AuPd/TiO_2-101(8.8%), suggesting a higher amount of oxygen vacancies on the surface of TiO_2-001. Such additional formation of oxygen vacancy might be attributed to the difference of formation energy of oxygen vacancy on the specific crystal facet of TiO_2, which sta-bilizes more oxygen vacancy on the surface of AuPd/TiO_2-001 [37]. In result, it explains why the binding energy of Ti 2p from TiO_2-001 (464.8 eV and 459.1 eV assigned to Ti $2p_{2/3}$ and $2p_{1/2}$) tends to be slightly lower than from TiO_2-101 (465.0 eV and 459.2 eV assigned to Ti $2p_{2/3}$ and $2p_{1/2}$). Moreover, oxygen vacan-cies were widely studied for its capability to stabilize metallic nanoparticles and promote alcohol oxidations by facilitating O_2 dissociation [38]. Furthermore in our study, the oxygen vacancies were suggested to be closely related to the enhanced activity for benzyl alcohol oxidation, which will be discussed in the part of cat-alytic performance measurement.

The surface atomic composition could also be obtained by XPS and the corresponding specific values were summarized in Table S2 in SI. Compared with the AuPd bulk composition determined by ICP-AES, it can be found that the Au and Pd concentra-tions on the surface of the AuPd/TiO_2-101 and AuPd/TiO_2-001 catalysts were higher than that of the bulk, which further proves that sol-immobilization method can effectively improve the sur-face exposure of AuPd nanoparticles in the catalyst. According to recent reports, the detection depth of XPS analysis for Au 4f and Pd 3d were ranged from 5.4 to 5.8 nm and from 4.6 to 5.0 nm, respectively [39]. However, the detected concentrations of Pd on the catalyst surface were higher than that of Au, as a result, the Au/Pd molar ratios were also lower than the nominal values, which indicates the enrichment of Pd species on the TiO_2 surface. The similar experimental phenomena were also observed by David et al. [40].

The particle size distribution of AuPd NPs on AuPd/TiO_2-001 and AuPd/TiO_2-101 was characterized by TEM. From Fig. 4, we can see AuPd nanoparticles were highly dispersed on their TiO_2 supports. According to the measurement results of 150 nanoparti-cles from the TEM, it is concluded that AuPd/TiO_2-001 and AuPd/ TiO_2-101 catalysts showed a similar Au-Pd particle size distribu-tion with the corresponding values of 3.3 ± 0.7 nm and 3.4 ± 0.7 n m, respectively. The standard deviation was calculated based on the mean size of nanoparticles, see Eq. (1) in SI. Therefore, it is con-firmed that the size distribution of AuPd NPs on TiO_2 is almost not affected by the exposed crystal facet of the carrier. Furthermore, to

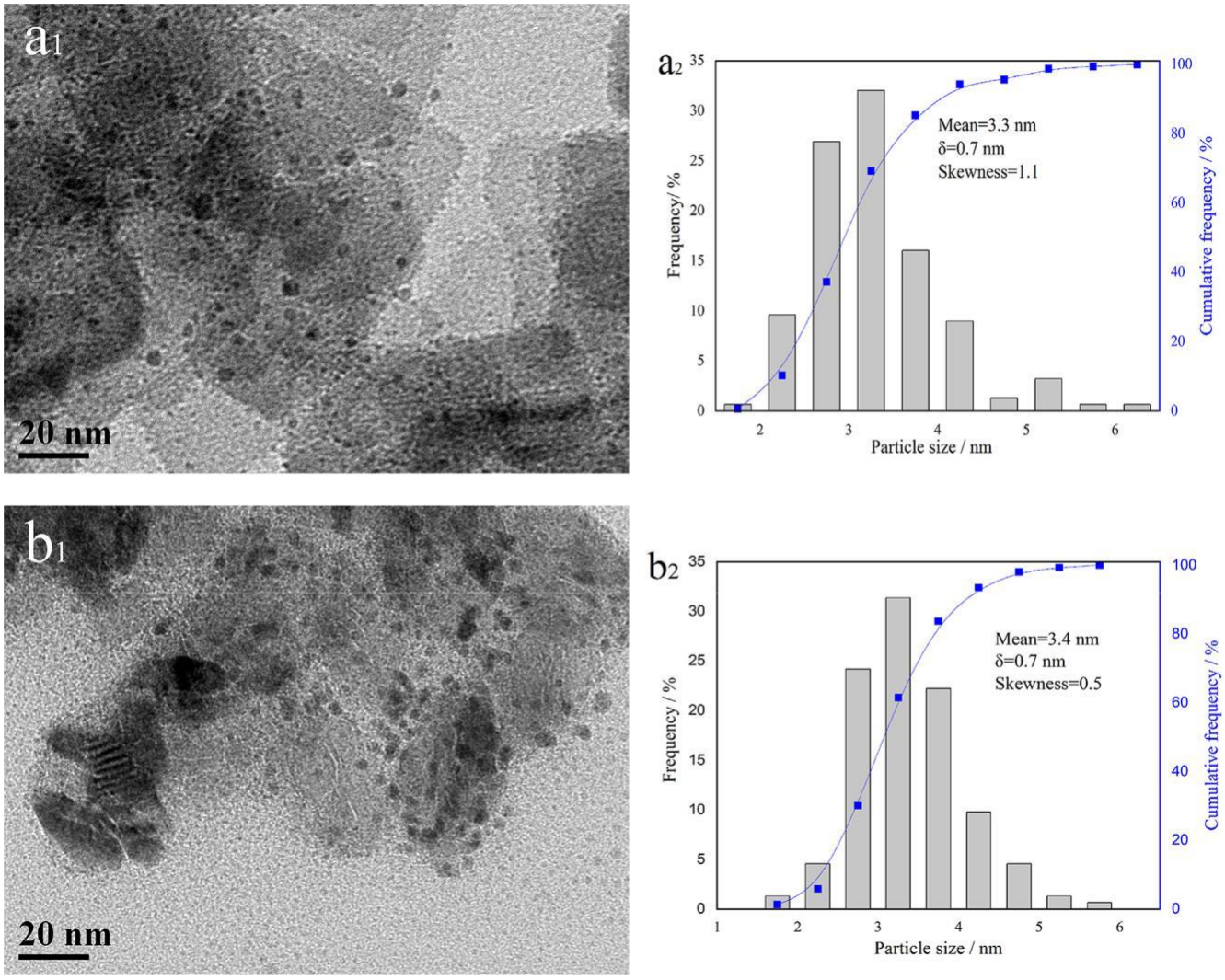

Fig. 4. TEM images and Au-Pd particle size distribution histograms of AuPd/TiO_2-001 and AuPd/TiO_2-101 catalysts.

determine the structure of AuPd NPs, STEM-EDS mapping was con-ducted for the solid catalysts, where signals of Au and Pd were obtained in the spectrum of energy at 2.2 keV and 3.0 keV, see Fig. S1 and S2 in SI. Also, the image showed that elements of Au and Pd are homogeneously scattered in the selected single nanoparticles in both AuPd/TiO_2-001 and AuPd/TiO_2-101, indicat-ing that Au and Pd atoms stay randomly alloyed in the present cat-alysts. To inspect the homogeneity of the formed bimetallic particles before immobilization, UV–vis absorption spectra were operated and the results are exhibited in Fig. S2 in SI, where no sur-face plasmon resonance peak were detected from the bimetallic AuPd colloids, suggesting the AuPd colloids were also alloyed before they get immobilized.

4. Catalytic performance measurement

Solvent free catalytic oxidation of benzyl alcohol was performed as a model reaction for testing the prepared AuPd/TiO_2 catalysts and their corresponding bare supports. Based on the experimental results in Fig. 5, we confirmed that AuPd alloy supported on TiO_2-001 showed higher activity than that supported on TiO_2-101. Addi-tionaly, AuPd/TiO_2-P25 was tested as well for the same reaction which displayed an activity between the other two catalysts. Along

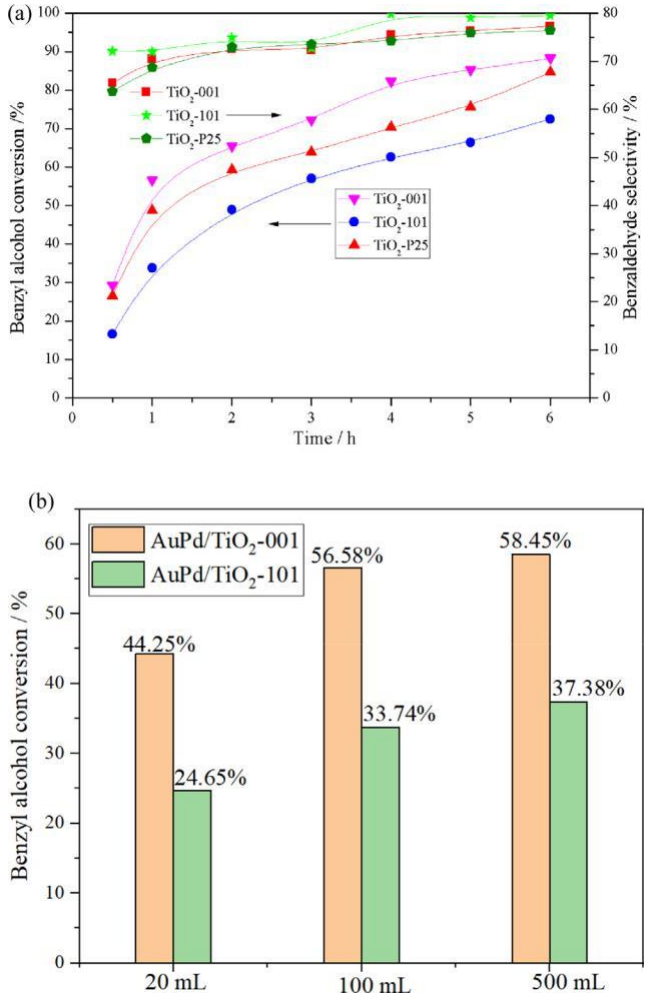

Fig. 5. Benzyl alcohol oxidation displays (a) conversion and benzaldehyde selec-tivity as a function of time achieved on AuPd/TiO_2-001, AuPd/TiO_2-101 and AuPd/ TiO_2-P25 catalysts; (b) conversion affected by particle size of AuPd nanoalloys. Reaction conditions: catalyst mass 30 mg, temperature 120 LC, benzyl alcohol 15 mL, O_2 0.3 MPa, stirring rate 1000 rpm.

a 6 h reaction, the benzyl alcohol conversion over AuPd/TiO_2-001 displayed ca 20% and 10% higher than AuPd/TiO_2-101 and AuPd/ TiO_2-P25 over time course respectively. Furthermore, each bare support was evaluated featuring negligible benzyl alcohol conver-sion of less than 1.2% over all the TiO_2 supports in this study, show-ing the supports alone are contributing little in the reaction. The higher catalytic activity of AuPd/TiO_2-001 might be correlated to the higher molar value of $O_a/(O_a + O_b)$ in AuPd/TiO_2-001 than that in AuPd/TiO_2-101, which was indicated by XPS characterization. As was reported, the more the surface oxygen vacancies O_a in the cat-alyst are, the higher the number of O_2 molecules are adsorbed onto the catalyst surface during oxidation reactions, which would greatly affect the catalytic performances because of the decreased reaction energy barrier [41]. Meanwhile it was also reported that these adsorbed oxygen atoms on the catalyst surface are intimately involved in benzyl alcohol oxidation due to the formation of alkoxy groups [42]. In regard to the product distribution, both catalysts showed a very high selectivity (over 70%) towards benzyl alde-hyde, which means the dehydrogenation of benzyl alcohol is the main reaction route over the TiO_2 supported AuPd catalysts while few disproportionation reactions of benzyl alcohol take place towards the production of toluene. Besides, the observed catalytic performance trends were not attributed to the nanoparticle size effect since the AuPd alloyed NPs represented comparable mean sizes between AuPd/TiO_2-001 (3.3 ± 0.7 nm) and AuPd/TiO_2-101 (3.4 ± 0.7 nm), as analyzed in Fig. 4. However, we did modify the AuPd NPs size distribution by using various volumes of distilled water (20 mL, 100 mL and 500 mL) for making the colloids, which was a well-known and commonly reported method [43]. The cata-lyst preparation details are provided in SI, along with TEM images and particles size distribution analysis (Fig. S4). It is conclusive that under the higher the concentration of dissolved AuPd precursors, the larger sized particles are generated. Namely, for AuPd/TiO_2-001, 20 mL (4.8 ± 1.0 nm) > 100 mL (3.3 ± 0.7 nm) > 500 mL (2.9 ± 0.5 nm); for AuPd/TiO_2-101, 20 mL (4.6 ± 0.5 nm) > 100 mL (3. 4 ± 0.7 nm) > 500 mL (2.6 ± 0.3 nm). Particle size effects towards catalytic activity are exhibited in Fig. 5b, where smaller particle size is favored in achieving a higher conversion of benzyl alcohol oxidation. The enhancement is over 10% in the catalyst made from colloids with 100 mL than that with 20 mL DI water, but it decreases in the catalyst made from more diluted colloids with 500 mL DI water. The result is consistent to literature [44].

Furthermore, AuPd/TiO_2-001 and AuPd/TiO_2-101 were recycled for 3 times in the same reaction for stability test. After each cycle, the used sample was washed with deionized water and acetone for surface cleaning, followed by drying at 110 LC overnight. Fig. 6 demonstrated that for both catalysts manifested a high durability with a decreased conversion of benzyl alcohol by only 5% for AuPd/TiO_2-001 and 8% for AuPd/TiO_2-101 after 3 cycles.

For the purpose of further clarifying the relationship between the catalytic performance and the structure, it is essential to com-pare the turnover frequency (TOF) values for the Au-Pd/TiO_2 cata-lysts with different facets exposed in solvent-free catalytic oxidation of benzyl alcohol. It is generally accepted that the TOF values could be obtained when the catalytic conversion is lower than 15.0%. Hence, the TOF values were measured after first 0.5 h of reaction with less amount of catalyst (20 mg). The calculation details and the corresponding results were summarized in Table S3 in SI. Apparently, the TOF value of AuPd/TiO_2-001 (28, 386 h^{-1}) was much higher than that of AuPd/TiO_2-101 (16,605 h^{-1}) under 0.3 MPa O_2 and 120 LC. It is found that the supe-rior AuPd/TiO_2-001 catalyst in this study achieved a higher TOF than those reported, i.e. Au-Pd-PVA/TiO_2 (10,300 h^{-1}) [45] and Au-Pd-GO/TiO_2 composites(10,400 h^{-1}), [44] measured under sim-ilar reaction conditions to ours, i.e. at 1 bar O_2 and 120 LC. Apart from mild conditions, it was reported that the partial pressure of

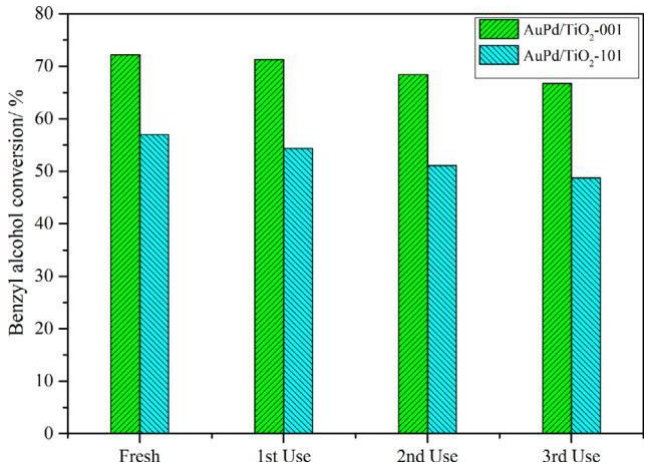

Fig. 6. The reuse of the AuPd/TiO2-001 and AuPd/TiO2-101 catalysts in benzyl alcohol oxidation under solvent-free condition. Reaction conditions: catalyst mass 30 mg, temperature 120 ℃, benzyl alcohol 15 mL, O_2 0.3 MPa, stirring rate 1000 rpm, 3 h.

O_2 has no effect on the reaction rate in benzyl alcohol oxidation, resulting in a similar TOF number when reactions were performed at higher pressure, i.e. 1% (Au + Pd)/TiO_2 (TOF: 15360 h^{-1}); 1% (Pd@Au)/TiO_2 (TOF: 19250 h^{-1}); 1% (Au@Pd)/TiO_2 (TOF: 17360 h^{-1}) at conditions of 10 bar O_2 and 120 ℃ [46]. Further com-parisons and discussions among AuPd with different supports in benzyl alcohol oxidation are provided in Table S3, from which the TOF values in this study can be recognized as one of the highest under the given reaction conditions.

5. Conclusion

In conclusion, AuPd/TiO_2-001 dominantly exposing {0 0 1} facets in its support had experimentally exhibited better catalytic perfor-mance in solvent-free benzyl alcohol oxidation than AuPd NPs immobilized on TiO_2 spindles with {1 0 1} facets preferentially exposed. The catalytic performance data and characterization results revealed that the catalytic activity in benzyl alcohol oxida-tion could be largely affected by the exposed facets of TiO_2 which tunes the number of available surface adsorbed oxygen. The enhanced catalytic performance of AuPd NPs supported on TiO_2 {0 0 1} facets was attributed to the nature of {0 0 1} facets with abundant oxygen vacancies and high surface energy. The present study demonstrated that apart from photocatalysis, the TiO_2 exposing specific facets also plays an important role in oxidative reaction without UV irradiation, which offer offers a remarkable way for the design of future heterogeneous catalysts and extends their application in conventional alcohol oxidation reactions.

Declaration of Competing Interest

The authors declare that they have no known competing finan-cial interests or personal relationships that could have appeared to influence the work reported in this paper.

Acknowledgment

The authors acknowledge with gratitude and appreciation financial support from the Natural Science Foundation of China (Nos. 21878200 and 21706271), the Natural Science Foundation of Shanxi Province (No. 201901D211582), and the China Postdoc-toral Science Foundation (No. 2019M653488).

References

[1] H. Li, F. Qin, Z. Yang, X. Cui, J. Wang, L. Zhang, J. Am. Chem. Soc. 139 (2017) 3513–3521.
[2] M. Du, G. Zeng, J. Huang, D. Sun, Q. Li, G. Wang, X. Li, ACS Sustainable Chem. Eng. 7 (2019) 9717–9726.
[3] J. Li, M. Li, H. Sun, Z. Ao, S. Wang, S. Liu, ACS Catal. 10 (2020) 3516–3525.
[4] D. Enache, J. Edwards, P. Landon, B. Solsona-Espriu, A. Carley, A. Herzing, M. Watanabe, C. Kiely, D. Knight, G. Hutchings, Science 311 (2006) 362–365.
[5] Y. Chen, H. Lim, Q. Tang, Y. Gao, T. Sun, Q. Yan, Y. Yang, Appl. Catal. A. Gen. 380 (2010) 55–65.
[6] Y. Hao, G. Hao, D. Guo, C. Guo, W. Li, M. Li, A. Lu, ChemCatChem 4 (2012) 1595–1602.
[7] X. Li, J. Feng, J. Sun, Z. Wang, W. Zhao, Nanoscale Res. Lett. 14 (2019) 1–9.
[8] M. Du, G. Zeng, C. Ye, H. Jin, J. Huang, D. Sun, Q. Li, B. Chen, X. Li, Mol. Catal. 483 (2020) 1–4.
[9] N. Reddy, U. Bharagav, M. Kumari, K. Cheralathan, M. Shankar, K. Reddy, T. Saleh, T. Aminabhavi, J. Environ. Manage. 254 (2020) 1–8.
[10] N. Reddy, V. Rao, M. Vijayakumar, R. Santhosh, S. Anandan, M. Karthik, M. Shankar, K. Reddy, N. Shetti, M. Nadagouda, T. Aminabhavi, Int. J. Hydrogen. Energy. 44 (2019) 10453–10472.
[11] N. Reddy, V. Rao, M. Kumari, R. Kakarla, P. Ravi, M. Sathish, M. Karthik, S. Inamuddin, Environ. Chem. Lett. 16 (2018) 765–796.
[12] K. Karthik, C.h. Reddy, K. Reddy, R. Ravishankar, G. Sanjeev, R. Kulkarni, N. Shetti, A. Raghu, J. Mater. Sci: Mater. Electron. 30 (2019) 20646–20653.
[13] S. Patil, P. Basavarajappa, N. Ganganagappa, M. Jyothi, A. Raghu, K. Reddy, Int. J. Hydrogen. Energy. 44 (2019) 13022–13039.
[14] C.h. Reddy, K. Reddy, N. Shetti, J. Shim, T. Aminabhavi, D. Dionysiou, Int. J. Hydrogen. Energy. 45 (2020) 18331–18347.
[15] K. Reddy, K. Nakata, T. Ochiai, T. Murakami, D. Tryk, A. Fujishima, J. Nanosci. Nanotechno. 10 (2010) 7951–7957.
[16] K. Kannan, D. Radhika, K. Sadasivuni, K. Reddy c, A. Raghu, Adv. Colloid. Interfac. 281(2020)1-12.
[17] V. Rao, N. Reddy, M. Kumari, P. Ravi, M. Sathish, K. Kuruvilla, V. Preethi, K. Reddy, N. Shetti, T. Aminabhavi, M. Shankar, Appl. Catal. B- Environ. 254 (2019) 174–185.
[18] P. Basavarajappa, S. Patil, N. Ganganagappa, K. Reddy, A. Raghu, C.h. Reddy, Int. J. Hydrogen. Energy. 45 (2020) 7764–7778.
[19] Y. Hong, X. Jing, J. Huang, D. Sun, T. Wubah, F. Yang, M. Du, Q. Li, ACS Sustain Chem. Eng. 2 (2014) 1752–1759.
[20] Q. Xiang, J. Yu, Chin. J. Catal. 32 (2011) 525–531.
[21] J. Yu, L. Qi, M. Jaroniec, J. Phys. Chem. C. 114 (2010) 13118–13125.
[22] D. Li, S. Chen, R. You, Y. Liu, M. Yang, T. Cao, K. Qian, Z. Zhang, J. Tian, W. Huang, J. Catal. 368, 163–171.
[23] Q. Shi, Y. Li, Y. Zhou, S. Miao, N. Ta, E. Zhan, J. Liu, W. Shen, J. Mater. Chem. A. 3 (2015) 14409–14415.
[24] J. Mao, L. Ye, K. Li, X. Zhang, J. Liu, T. Peng, L. Zan, Appl. Catal. B. Environ. 144 (2014) 855–862.
[25] X. Pan, N. Zhang, X. Fu, Y. Xu, Appl. Catal. A. Gen. 453 (2013) 181–187.
[26] X. Han, Q. Kuang, M. Jin, Z. Xie, L. Zheng, J. Am. Chem. Soc. 131 (2009) 3152– 3153.
[27] L. Kesavan, R. Tiruvalam, M. Rahim, M. Saiman, D. Enache, R. Jenkins, N. Dimitratos, J. Lopez-Sanchez, S. Taylor, D. Knight, C. Kiely, G. Hutchings, Science 331 (2011) 195–199.
[28] M. Liu, L. Piao, W. Lu, S. Ju, L. Zhao, C. Zhou, H. Li, W. Wang, Nanoscale 2 (2010) 1115–1117.
[29] Y. Cao, Q. Li, C. Li, J. Li, J. Yang, Appl. Catal. B: Environ. 198 (2016) 378–388.
[30] X. Li, J. Feng, M. Perdjon, R. Oh, W. Zhao, X. Huang, S. Liu, Appl. Sur. Sci. 505 (2020) 1–8.
[31] J. Xu, T. White, P. Li, C. He, J. Yu, W. Yuan, Y. Han, JACS 132 (2010) 10398– 10406.
[32] N. Hayashi, Y. Sakai, H. Tsunoyama, A. Nakajima, Langmuir 30 (2014) 10539– 10547.
[33] Z. Li, F. Gao, O. Furlong, W. Tysoe, Surf. Sci. 604 (2010) 136–143.
[34] J. Sanchez, N. Dimitratos, C. Hammond, G. Brett, L. Kesavan, S. White, P. Miedziak, R. Tiruvalam, R. Jenkins, A. Carley, D. Knight, C. Kiely, G. Hutchings, Nat. Chem. 3 (2011) 551–556.
[35] Z. Yin, M. Chi, Q. Zhu, D. Ma, J. Sun, X. Bao, J. Mater. Chem. A. 1 (2013) 9157– 9163.
[36] B. Pawelec, A. Venezia, V. Parola, E. Cano-Serrano, J. Campos-Martin, J. Fierro, Appl. Sur. Sci. 242 (2005) 380–391.
[37] H. Li, Y. Guo, J. Robertson, J. Phys. Chem. C 119 (2015) 18160–18166.
[38] C. Xiao, L. Zhang, H. Hao, W. Wang, ACS Sustainable Chem. Eng. 7 (2019) 7268– 7276.
[39] C. Olmas, L. Chinchilla, E. Rodrigues, J. Delgado, A. Hungría, G. Blanco, M. Pereria, J. Órfão, J. Calvino, X. Chen, Appl. Catal. B. Environ. 197 (2016) 222– 235.
[40] M. Khawaji, D. Chadwick, Catal. Today 334 (2019) 122–130.

[41] S. Saad, N. Alias, M. Ramli, N. Abdullah, N. Malek, M. Rosli, A. Umar, RSC Adv. 10 (2020) 16886–16891.
[42] A. Savara, I. Rossetti, C. Thaw, L. Parati, A. Villa, ChemCatChem 8 (2016) 2482–2491.
[43] X. Liang, Z. Wang, C. Liu, Nanoscale Res. Lett. 5 (2010) 124–129.
[44] C. Olmos, L. Chinchilla, A. Villa, J. Delgado, A. Hungría, G. Blanco, L. Prati, J. Calvino, X. Chen, J. Catal. 375 (2019) 44–55.
[45] J. Wang, S. Kondrat, Y. Wang, G. Brett, C. Giles, J. Bartley, L. Lu, Q. Liu, C. Kiely, G. Hutchings, ACS Catal. 5 (2015) 3575–3587.
[46] M. Khawaji, D. Chadwick, ChemCatChem 9 (2017) 4353–4363.